Nanoscale Changes in Collagen are Reflected in Physical and Mechanical Properties of Bone at the Microscale in Diabetic Rats

Max A Hammond [a], Maxime A Gallant [b], David B Burr [b, d], Joseph M Wallace [a, c, d]

[a] Weldon School of Biomedical Engineering, Purdue University, West Lafayette, IN
[b] Department of Anatomy and Cell Biology, Indiana University School of Medicine, IN
[c] Department of Orthopaedic Surgery, Indiana University School of Medicine, IN
[d] Department of Biomedical Engineering, Indiana University-Purdue University at Indianapolis, IN

*Corresponding Author:
Dr. Joseph M. Wallace
Indiana University-Purdue University at Indianapolis
Department of Biomedical Engineering
723 W Michigan St. SL220D
Indianapolis, IN 46202

Phone: (317) 274-2448
Fax: (317) 278-2455
E-mail: jmwalla@iupui.edu

Highlights:

- Multiscale analysis of changes in diet-induced Type 2 diabetes in rats
- Atomic Force Microscopy, Raman Spectroscopy, Reference Point Indentation used
- Nanoscale morphology, mineral:matrix ratios, microscale mechanics altered
- Colocalized Raman and Reference Point Indentation were significantly correlated
- Mineral:matrix changes reflect stiffening of matrix, possibly due to glycation

ABSTRACT

Diabetes detrimentally affects the musculoskeletal system by stiffening the collagen matrix due to increased advanced glycation end products (AGEs). In this study, tibiae and tendon from Zucker diabetic Sprague-Dawley (ZDSD) rats were compared to Sprague-Dawley derived controls (CD) using Atomic Force Microscopy. ZDSD and CD tibiae were compared using Raman Spectroscopy and Reference Point Indentation (RPI). ZDSD bone had a significantly different distribution of collagen D-spacing than CD (p=0.015; ZDSD n=294 fibrils; CD n=274 fibrils) which was more variable and shifted to higher values. This shift between ZDSD and CD D-spacing distribution was more pronounced in tendon (p<0.001; ZDSD n=350; CD n=371). Raman revealed significant increases in measures of bone matrix mineralization in ZDSD (PO_4^{3-} ν1/Amide I p=0.008; PO_4^{3-} ν1/CH_2 wag p=0.047; n=5 per group) despite lower bone mineral density (aBMD) and ash fraction indicating diabetes may preferentially reduce the Raman signature of collagen. Decreased indentation distance increase (p=0.010) and creep indentation distance (p=0.040) measured by RPI (n=9 per group) in ZDSD rats suggest a matrix more resistant to indentation under the high stresses associated with RPI at this length scale. There were significant correlations between Raman and RPI measurements in the ZDSD population (n=18 locations) but not the CD population (n=16 locations) indicating that while RPI is relatively unaffected by biological noise, it is sensitive to disease-induced compositional changes. In conclusion, diabetes in the ZDSD rat causes changes to the nanoscale morphology of collagen that result in compositional and mechanical effects in bone at the microscale.

KEYWORDS

1. INTRODUCTION

Diabetes is a widespread problem affecting over 25.8 million people in the United States alone (8.3% of the US population), with 90-95% of cases in adults being type 2 diabetes mellitus (non-insulin-dependent diabetes mellitus, T2DM) [1]. T2DM has detrimental impacts on multiple organ systems including the renal, circulatory and nervous systems. There are destructive effects on the musculoskeletal system as well, although studies are limited in comparison to other systems. T2DM patients have a higher fracture risk despite having a higher BMD [2]. The increased fracture risk can partially be explained by increased fall risk as a result of complications from T2DM such as peripheral neuropathy and impaired vision [3]. Reductions in bone quality may also play a role, and while studies in humans are limited, intrinsic mechanical properties of bone in animal models of diabetes are reduced [4, 5].

The reduction in bone quality with T2DM is likely the result of chronic hyperglycemia increasing the presence of advanced glycation end products (AGEs) [6] which form when reducing sugars react with free amino groups in proteins. Permanent non-enzymatic crosslinks in collagen form when sugars react with Lysine or Hydroxylysine residues and the subsequent Amadori product reacts with neighboring Lysine or Arginine residues [7]. In contrast to enzymatic crosslinks which are beneficial to bone quality and are produced in a tightly regulated process, non-enzymatic crosslinks form randomly [7]. The non-enzymatic crosslinks presumably reduce bone quality by inhibiting collagen fibril slip [8-10], which is theorized to be a major toughening mechanism for bone at higher length scales [10, 11]. However, few studies have directly investigated the collagen ultrastructure in diabetic tissues and made attempts to link these changes to compositional and mechanical changes at higher length scales.

1   The purpose of this work was to study the nanoscale morphology of Type I collagen in

2   mineralized and non-mineralized tissues from normal and diabetic rats, and to investigate

3   possible effects of diabetes on mineral chemistry and tissue mechanical properties. A novel

4   mechanical testing technique known as Reference Point Indentation (RPI) was utilized to probe

5   the mechanical effects at the microscale. Raman spectroscopy was used to investigate alterations

6   to the chemical composition. In a subset of samples, Raman spectroscopy was co-localized with

7   RPI to investigate correlations between composition and the RPI device BioDent Hfc. We

8   hypothesized that diabetes-induced effects would be detected through alterations in the nanoscale

9   morphology of collagen, changes in bone Raman signatures, increased matrix stiffness and

10   increased indentation depth increase in diabetic rats.

11

2. MATERIALS AND METHODS

2.1 Animals

Male Sprague-Dawley-derived control rats (CD: Charles River Laboratory, Wilmington, MA) and male Zucker diabetic Sprague-Dawley rats (ZDSD: PreClinOmics, Indianapolis, IN) were used with prior approval. At 17 weeks of age, all animals were switched from regular chow (Purina 5008) to a high fat test diet (Test diet 5SCA) for two weeks to induce T2DM in the ZDSD rats generally by 18 weeks of age. At 19 weeks of age, all animals were switched back to regular chow until sacrifice by CO_2 inhalation at 30 weeks of age. Weekly glucose monitoring following the initiation of the high fat diet and blood serum analysis at 30 weeks of age verified that each ZDSD rat maintained a blood glucose level that was above the diabetic threshold (>250 mg/dl) after returning to regular chow. Following sacrifice, right tibiae and tails were harvested, wrapped in saline-soaked gauze and stored at -20°C until needed (n=9 per group).

2.2 Atomic Force Microscopy

From the tibia (n=4 per group), a 12 mm section of the diaphysis surrounding the tibia-fibula junction (TFJ) was removed using a low-speed sectioning saw, mounted anterior-side up to a steel disk with cyanoacrylate glue, and polished using a 3 μm diamond suspension to create a flat face parallel to the anterior surface. Each section was treated for 20 minutes with 0.5M ethylenediaminetetraacetic acid (EDTA) at a pH of 8.0 followed by sonication for 5 minutes in water. This process was repeated 4 times. Samples were imaged using a BioScope Catalyst AFM in peak force tapping mode (Bruker, Santa Barbara, CA). Images were acquired from 4-5 locations in each bone using a silicon cantilever with a silicon probe (tip radius ~ 8 nm). At each location, 10-15 fibrils were analyzed in 3.5 μm x 3.5 μm error images (~70 fibrils per bone)

1   using 2D Fast Fourier Transforms (2D FFT) as previously described [12-15]. Briefly, 2D FFTs

2   were performed on individual fibrils and the first harmonic peak from the power spectrum was

3   used to determine the D-periodic spacing for that fibril.

4   From the tail of each rat (n=4 per group), ~75 mm lengths of individual tendon fascicles

5   were removed and placed in phosphate buffered saline (PBS). Each fascicle was placed on a

6   glass slide and gently flattened with curved forceps. The fascicle was allowed to dry just long

7   enough to adhere to the glass before imaging in air. Samples were imaged using a BioScope

8   Catalyst AFM in peak force tapping mode. For at least three fascicles per tail sample, images

9   were acquired from 1-2 locations using a silicon nitride cantilever with a silicon probe (tip radius

10   ~ 2 nm). At each location, 10-15 fibrils were analyzed in 5 μm x 5 μm error images (~90 fibrils

11   per tail) using 2D FFTs.

12   *2.3 Raman Spectroscopy*

13   From the remaining tibia (n=5 per group), a 12 mm section surrounding the TFJ was

14   created, mounted anterior-side up to a steel disc and stripped of the periosteum along the

15   periosteal surface by scraping with a scalpel. Reference marks were added to the proximal and

16   distal ends of the section. The relative distance between each reference mark was recorded to

17   allow for registration with Reference Point Indentation (RPI). Five locations were imaged, ~1-2

18   mm apart, along the native anterior surface of bone while the rest of the bone was submerged in

19   a PBS bath. Raman spectroscopy was performed using a LabRAM HR 800 Raman Spectrometer

20   (HORIBA Jobin Yvon, Edison, NJ) with an integrated BX41 microscope (Olympus, Tokyo,

21   Japan). A 660 nm laser was focused on the surface using a 50X objective (NA=0.75) to a spot

22   size of ~10 μm and five 20 sec acquisitions were averaged at each location. After a five point

linear baseline correction in LabSpec 5 (HORIBA Jobin Yvon), OriginPro 8.6 (OriginLab,

Northampton, MA) was used to fit a single Gaussian peak to the phosphate PO_4^{3-} ν1 peak and to

integrate the peaks corresponding to PO_4^{3-} ν1, CO_3^{2-} ν1, Amide III, CH_2 wag, and the Amide I

envelope (Figure 1). Wavenumber ranges for each peak were kept standard across all spectra and

were chosen based on previous literature [16, 17] and to reduce contributions of either other

peaks or noise. Type B carbonate substitution was found by the band area ratio of CO_3^{2-} ν1/

PO_4^{3-} ν1. The mineralization of the matrix was determined by the band area ratios PO_4^{3-}

ν1/Amide I, PO_4^{3-} ν1/ CH_2 wag, and PO_4^{3-} ν1 /Amide III. Crystallinity/maturity was determined

by 1/full width at half maxima (FWHM) of the PO_4^{3-} ν1 peak.

2.4 Reference Point Indentation

RPI was performed using a BioDent Hfc (Active Life Scientific, Santa Barbara, CA) with

Bone Probe 3 (BP3) in the region proximal to where the 12 mm sections were excised for either

Raman or AFM imaging (n=9 per group). Starting at least 2 mm from the distal end of the

section, five locations 1-2 mm apart were indented using the Bone Probe 3 (BP3) along the

anterior surface of the bone while in a PBS bath. Ten cycles of a 5 N indentation force were

applied at a frequency of 2 Hz. A custom Matlab (Mathworks, Natick, Massachusetts) program

was used to calculate the 1st cycle indentation distance (ID 1st), 1st cycle energy dissipation (ED

1st), 1st cycle unloading slope (US 1st), 1st cycle creep indentation distance (CID 1st), indentation

distance increase (IDI), total indentation distance (TID), total energy dissipation (ED Tot),

average creep indentation distance (CID Avg), average energy dissipation from cycles 3-10 (ED

Avg), and average unloading slope (US Avg) [18]. At the start of each indentation day, a

standard block of polymethyl methacrylate (PMMA) was indented with the above protocol to

serve as an internal standard.

In a subset of bones (n=4 per group), additional RPI testing was performed in order to regionally co-localize indents with previously acquired Raman spectra (n=16 locations in CD, n=18 locations in ZDSD). Due to the update to the BioDent Hfc from the previous Biodent system mid-study, one bone from each group was excluded from the original five per group for Raman. In addition, six locations between both groups were slightly off center causing the reference probe to slip during testing and were excluded yielding n=16 and n=18 locations in CD and ZDSD, respectively. Using a custom stage and the reference marks at the end of each section, a VMS-004D microscope (Veho, Hampshire, UK) mounted to the BioDent, and the relative geometry between each location and the reference marks, RPI measurements were registered to within approximately 200-400 μm of the Raman locations. Indentations were performed using the same indentation protocol as above while the samples were kept hydrated in a PBS bath.

2.5 Statistical Analysis

Mean comparisons between CD and ZDSD were analyzed with a Student's t-test. Locations within the same sample were averaged to yield a single sample value for mean comparisons between groups. If normality was violated (determined by a Shapiro–Wilk test with a $p < 0.05$), a Wilcoxon rank-sum test was performed. If homoscedasticity was violated (determined by a Brown-Forsythe test with a $p < 0.05$), a t-test was performed using the Satterthwaite approximation. In the RPI dataset with n=9 per group, the day indentation was performed was a suspected nuisance factor. To overcome the increased variability associated with this factor, blocking was implemented with a two-way ANOVA with indentation day as a fixed effect for all RPI parameters for mean comparison. Violations of normality or homoscedasticity were overcome with a Poisson's transformation when needed. To compare the

1   distribution of fibril D-spacing from AFM, a Kolmogorov–Smirnov test (KS test) was employed.

2   For examining correlations between the co-localized Raman and RPI measures, a Pearson

3   product-moment correlation was calculated for each group and tested for significance. For all

4   tests, two-sided tests were used and $p < 0.05$ was considered significant. SAS 9.3 (SAS, Cary,

5   NC) was used to perform all tests. All data are presented as mean ± standard deviation (SD).

6

3. RESULTS

3.1 Animal Information

All ZDSD rats had a blood glucose level above 250 mg/dl while no CD rat was above 250 mg/dl. As seen in Table 1, ZDSD had a significantly lower body weight (p<0.001), a significantly higher glucose level (p<0.001), and a significantly higher percentage of glycated hemoglobin (Hb1Ac; p<0.001) than CD. ZDSD had lower mineralization as measured by aBMD from DEXA (p<0.001) and ash fraction (p<0.001) compared to CD (Table 1).

3.2 Atomic Force Microscopy

Measurements within each sample were averaged to yield the mean fibril spacing for that sample. In bone, the overall mean D-spacing was 66.1 ± 0.8 nm for CD and 66.5 ± 1.5 nm for ZDSD with no statistical difference between group means (p=0.584). Fibril D-spacing distributions were significantly different between groups (Figure 2a, n=274 in CD, n=294 in ZDSD, p=0.015). In tendon, the overall mean D-spacing was 68.4 ± 0.2 nm for CD and 68.6 ± 1.2 nm for ZDSD with no statistical difference between group means (p=0.699). Fibril D-spacing distributions were significantly different between groups (Figure 2b, n=371 in CD, n=350 in ZDSD, p<0.001). While mean D-spacing was not different between groups in either tissue type, ZDSD had a significantly different distribution of D-spacing values in both tissues indicating that collagen morphology is altered in this model of T2DM.

3.3 Raman spectroscopy

Mineral chemistry was not different between groups for either crystallinity/maturity (0.0545 ± 0.001 for CD and 0.0548 ± 0.001 for ZDSD, p=0.492) or type B carbonate substitution

(0.246 ± 0.016 for CD and 0.257 ± 0.011 for ZDSD, p=0.260). As seen in Figure 3, PO_4^{3-} $v1$/Amide I and PO_4^{3-} $v1$/ CH_2 wag were significantly increased in ZDSD (p=0.008 and p=0.047, respectively) while PO_4^{3-} $v1$/Amide III maintained the same trend but failed to reach significance (p=0.064).

3.4 Reference Point Indentation

Using the BioDent Hfc system and a custom Matlab code [18], ten parameters were extracted from the cyclic indentation force displacement curves and of these ten, the only two that were significantly different between ZDSD and CD were IDI and CID 1st (Table 2). IDI and CID 1st were significantly decreased by 8.8% and 9.7% from CD, respectively, in ZDSD. The effect of indentation day was successfully blocked and its effect was significant at the p<0.001 level for all parameters except Avg CID and Avg ED which were significant at the p<0.05 level.

3.5 Correlations between Raman Spectroscopy and Reference Point Indentation

Pearson product-moment correlations were calculated for each group to avoid correlations being driven by distinct population differences between CD and ZDSD, but at the cost of reduced degrees of freedom. In the CD group, all correlations were weak and nonsignificant. In the ZDSD group, there were several significant correlations between Raman and RPI (Table 3). Type B carbonate substitution had significant negative correlations with ID 1st, ED 1st, TID, and ED Tot. All three parameters used to capture relative mineralization of the matrix (PO_4^{3-} $v1$/Amide I, PO_4^{3-} $v1$/CH_2 wag, and PO_4^{3-} $v1$/Amide III) had significant positive correlations with ID 1st, ED 1st, TID, and ED Tot. Most correlations in ZDSD compared to CD were much stronger and in most cases in the reverse direction as highlighted by the drastically different correlations between ED 1st and PO_4^{3-} $v1$/Amide I (Figure 4).

4. DISCUSSION

This study investigated the morphological, chemical, and mechanical effects of a T2DM condition in the ZDSD rat. The ZDSD rat gradually develops overt hyperglycemia due to dietary manipulation, as opposed to the leptin receptor defect in ZDF or chemical treatment with streptozotocin (STZ), more closely mimicking the conditions of T2DM in humans [19]. While it is widely believed that AGEs are the driving mechanism behind changes observed in bone from T2DM patients and animal models of the disease [19], AGE levels were not quantified here but the early glycation product Hb1Ac was significantly increased over 2.5 times that of CD (Table 1). However, Sprague-Dawley rats treated with STZ [20] , spontaneously diabetic WBN/Kob rats [21], and spontaneously diabetic BB/Wor/Mol\BB rats [22] all indicate that rodent models of diabetes have significantly increased AGE accumulation in bone [20, 21] and in tendon [22]. Therefore, this study was designed under the assumption that AGE accumulation is also present in the bones of ZDSD rat.

D-spacing changes have been observed with estrogen deficiency [12, 13] and with genetic changes in collagen leading to Osteogenesis Imperfecta [14, 23]. Changes in collagen under these disease conditions are not restricted to bone [13, 23]. No differences in D-spacing distribution were noted between different tissue types in healthy mice [24], or between the bones of healthy male and female mice (unpublished result). Alternatively, differences in D-spacing may arise from strain specific effects due to the development of the ZDSD model from lean Zucker diabetic fatty (ZDF) *fa*/+ and Sprague-Dawley derived parent strains. However, comparing mixed background mice to a parent strain from two previous studies did not indicate strain specific changes in D-spacing after accounting for different system calibrations. Therefore, we are confident that the structural changes in collagen in the bone and tendon of diabetic rats

1   noted here are real manifestations of the disease. In bone, the D-spacing distribution is wider and

2   shifted higher in ZDSD as previously observed by Odetti in the tendons of another diabetic rat

3   model [22]. For the CD bone fibril population, 70% of all fibrils fell within the mean ± 1 SD

4   (63.6 nm to 68.6 nm) while only 67% of the ZDSD fibrils fell within this same range. The ZDSD

5   population was shifted to higher D-spacings, with 17% of fibrils above this range versus 14% in

6   CD fibrils. In order to separate the impact of mineralization from the D-spacing analysis, tendon

7   fibrils from each group were also investigated to verify that observed shifts in the ZDSD

8   population were inherent to collagen and not due to mineral or the interaction between organic

9   and inorganic components. The wider and higher-shifted distributions in ZDSD bone were more

10   pronounced in tendon as can be clearly observed in Figure 2. In CD tendons, almost 74% of all

11   fibrils fall within the mean ± 1 SD (67.3 nm to 69.4 nm) while only 55% of the ZDSD fibrils fall

12   within this same range. The ZDSD tendon fibrils were shifted higher, with 27% of fibrils above

13   this range versus 12% in CD fibrils. The shifts in bone were more subtle, likely due to the

14   presence of intrafibrillar mineral masking the dramatic effect observed in the non-mineralized

15   tendon collagen fibrils.

16   Altered D-spacing was likely driven by AGE-induced non-enzymatic crosslinks within

17   the collagen matrix, and although pentosidine was not directly measured in this study, it has been

18   shown to increase in other rat models of diabetes [20-22]. These non-enzymatic crosslinks could

19   induce internal stress within the collagen matrix causing fibrils to locally unwind or whole fibrils

20   to stretch/compress, resulting in the D-spacing changes here and the previously altered radius

21   and gap depth observed [22]. Altered collagen morphology could affect tissue mechanics

22   independently or in addition to overall collagen matrix stiffening and altered mineralization

23   nucleation and growth. Although a previous study did not report changes in ovine bone due to *in*

13

vitro glycation [25], other studies study showed shifts in both diabetic [22] and glycated samples [8, 22]. We observed shifts in both bone and tendon that were consistent with the latter studies supporting our conclusion that collagen nanoscale morphology is altered as a manifestation of diabetes and this is likely due to the presence of AGEs.

Ash fractions and bone mineral density measurements performed on femora from the animals used in this study revealed lower mineralization in ZDSD samples (Table 1). However, Raman spectroscopy revealed an increase in matrix mineralization based on all three mineral/matrix metrics here (Figure 3). This discrepancy could be attributed to differences between sampling volume for the two techniques. Confocal Raman microscopy was largely restricted to the first ~50 μm in depth on the surface whereas ash weight fractions were a global measurement of the entire bone. Another possibility is that as a consequence of AGE-induced crosslinks, the vibrational freedom of the collagen structure was reduced thereby decreasing the Raman signatures of the matrix (Amide I, Amide III, and CH_2 wag bands). If AGEs reduce matrix band signatures, thereby increasing mineral to matrix parameters, the greatest change would be expected in the PO_4^{3-} ν1/Amide I ratio and the mildest effect in PO_4^{3-} ν1/Amide III because of Amide I's sensitivity and Amide III's relative stability [26]. This expected trend was seen in the data presented here. Experiments are underway to verify that the increase in mineral to matrix ratios observed here were due to the presence of AGEs. The potential reduction of the matrix bands in bone caused by AGEs was an important finding because as in other tissues [27, 28], Raman spectroscopy could be developed as means to validate the presence of AGEs in bone without the destructive processing of traditional colorimetric [29] or mass spectroscopy-based assays [30].

The lower maximum indentation forces used here (5 N versus the previously used 10 N) may be an important reason why previous RPI data in ZDSD femora and L3 vertebral bodies showed a significant increase in IDI [31] compared to our observed decrease in the tibiae. Decreasing indentation force from 10 N to 5 N reduces indentation depth which presumably indents less bone that was formed before the initiation of the diabetic condition. The lower IDI suggests that the matrix of the ZDSD bones is more resistant to indentation, presumably due to the AGE-induced crosslinks. The cyclic indentation used by RPI likely captures elastic deformation, plastic deformation, and fracture toughness. The changes observed here are likely due to a combination of increased resistance to plastic deformation and altered fracture toughness because metrics related to stiffness, i.e. resistance to elastic deformation, are not changed as seen in Table 2 for US 1st and Avg US. The increased resistance to plastic deformation in ZDSD is supported by the decrease in CID 1st and the nonsignificant trends in CID, ID 1st, TID, ED 1st, supporting that ZDSD resists plastic deformation and indentation better than CD at this length scale. AGEs are shown to increase stiffness of demineralized collagen matrix [29], presumably by reducing collagen fibril slip [8-10] which is believed to be a major intrinsic toughening mechanism in bone [11]. Reduced fibril slip may account for the resistance to indentation observed here at the microscale and likely influences the bone's macroscale fracture toughness.

The disparity between length scales and the abnormally high levels of stress induced by RPI could explain why a diabetic model with known decreases in failure force and stiffness using traditional bending tests [31] could exhibit properties indicative of a stiffer bone matrix using RPI. Only the outer 40-60 μm of the cortex in a ~100 μm area is investigated with the BioDent system compared to a several millimeter cross section of the whole bone using bending.

RPI also exerts very high stresses on the bone in the range of 10 GPa-690 MPa from indentation distances 10-40 μm compared to the 200 MPa maximum bending stresses from traditional tests [32]. These major dissimilarities could explain the differences observed between RPI and traditional bending tests as the ZDSD bone benefits from reduced fibril slip to resist indentation using RPI but the loss of this intrinsic toughening mechanism [11] drives the reduced mechanical properties typically associated with AGE accumulation observed at higher length scales and lower stresses [33].

RPI was used to assess the effects of the diabetic condition on indentation parameters in the proximal end of the tibia. Testing for this portion of the study took place over a three day period, but all indentations used the same probe assembly. During these indentations, the IDI of a standard PMMA block was used as a system check at the start of each day. It was noted that IDI was reduced in the PMMA sample for the last day. This effect was likely due to the probe nearing the end of its 150 indent lifespan. For the analysis of this set of RPI data, the indentation day was included as a fixed effect on the RPI parameters. Examining the data from all indentations confirmed that the changes occurred uniformly across all samples indented on that day. If the data from the last day were removed yielding n=6 per group, the percentage change between groups for all parameters was uniformly shifted up by 1-2% with slightly higher p-values for CID 1st (p=0.037) and IDI (p=0.068) attributable to the lower sample size. To minimize the potential for this effect in the future, care should be taken to indent over as few of days as possible and to monitor the lifespan of the probe assembly.

RPI is an emerging technique in bone research, but the mechanical parameters associated with the technique can be difficult to interpret. Although indentation distance increase has been found to inversely correlate with toughness [31], correlations with other established techniques

1   in bone research such as Raman are needed. It is clear that while Raman and RPI were not

2   correlated in CD animals, there were many strong and significant correlations in ZDSD animals

3   (Table 3). The lack of parity between CD and ZDSD as demonstrated in Figure 4 indicates that

4   RPI is largely unaffected by biological variation in normal tissue but proportionally reflects

5   compositional changes due to variations of disease severity. The strong relationships between the

6   Raman parameters affected by the possible increased AGE accumulation and RPI parameters

7   indicate that RPI might reveal changes associated with level of glycation, opening new research

8   avenues utilizing this novel technique. However, the small sample size (n=4 per group) for the

9   distal tibiae sections did not allow for mean comparison between groups to verify these changes.

10   The correlations to RPI for CO_3^{2-} ν1/ PO_4^{3-} ν1 in ZDSD demonstrated that RPI is sensitive to

11   subtle changes in mineral chemistry.

12   As opposed to the approach taken for indentations performed in the proximal tibia, day of

13   indentation was not considered for the correlation analysis in the distal tibia. On the three days of

14   indentation used for the correlation analysis, no differences were noted in the standard PMMA

15   indentations. The effect noted in the proximal tibia was likely absent here because the indents at

16   these two locations were performed on different days. Additionally, the probe assembly used for

17   the correlation analysis was different than the probe assembly used for the group analysis and the

18   total number of indents for the correlations was less than half of the total number of indents for

19   comparisons between groups. A potential limitation of our correlation analysis was that our

20   locations were only co-localized to within 200-400 μm of each other due to registration

21   difficulties while visualizing the reference marks during RPI. Despite this spatial co-localization

22   error, the many highly significant and reasonably strong correlations in ZDSD suggest that

1   Raman and RPI are regionally correlated in this disease model and this correlation could

2   potentially be strengthened with increased spatial resolution in the co-localization.

3

5. CONCLUSIONS

In the ZDSD model of T2DM, the nanoscale morphology of Type I collagen was altered in bone and tendon. RPI detected mechanical effects at the microscale from diabetes suggests a matrix more resistant to plastic deformation presumably due to non-enzymatic crosslinks toughening the matrix against the high stresses caused by RPI. Reductions in the mineral to matrix band area ratios as measured by Raman spectroscopy may be able to detect the stiffening of the collagen matrix and should be explored as a possible test to verify the presence of AGEs in bone and other tissues. Raman spectroscopy and RPI had many strong correlations in ZDSD bone but not in CD samples indicating RPI metrics are a function of disease-induced compositional changes but are largely unaffected by biological noise in healthy tissues. These correlations will be explored further in future studies. Diabetes in the ZDSD rat causes morphological changes to the collagen matrix which are reflected in the composition and mechanics of the tissue.

6. ACKNOWLEDGEMENTS

FIGURE CAPTIONS

Figure 1. Band area ratios for Raman spectroscopy. The PO_4^{3-} v1 peak was fit with a Gaussian curve centered on ~960 cm^{-1}. Each peak's area was found by integrating from 930-980 cm^{-1} for the PO_4^{3-} v1 peak, from 1055-1090 cm^{-1} for the CO_3^{2-} v1 peak, from 1220-1300 cm^{-1} for the Amide III peak, from 1410-1490 cm^{-1} for CH$_2$ wag peak, and from 1550-1720 cm^{-1} for the Amide I envelope. Band area ratios were calculated from the integrated area. Crystallinity was found as the inverse of the FWHM from the fitted PO_4^{3-} v1 peak.

Figure 2. Cumulative distribution functions for CD and ZDSD in bone and tendon. ZDSD had significantly different distributions of collagen D-spacing in bone (n=274 in CD, n=294 in ZDSD, p=0.015) and tendon (n=371 in CD, n=350 in ZDSD, p<0.001) compared with CD rats. The ZDSD distribution is wider and shifted higher in both tissues with differences more pronounced in tendon.

Figure 3. Mineral to matrix ratios increase in ZDSD. PO_4^{3-} v1/Amide I was significantly increased (p=0.008) by a margin nearly double that of PO_4^{3-} v1/CH$_2$ wag and PO_4^{3-} v1/Amide III. PO_4^{3-} v1/CH2 wag was significantly increased (p=0.047) while PO_4^{3-} v1/Amide III was not significantly increased (p=0.064). n=5 per group * p<0.05

Figure 4. ED 1st to PO_4^{3-}/Amide I correlation. The ZDSD and CD populations have markedly different correlations. ZDSD PO_4^{3-}/Amide I had a significant moderately strong positive correlation with 1st cycle energy dissipation (n=18, R^2=0.625, p<0.001) whereas CD had a mild negative and non-significant correlation (n=16, R^2=0.168, p=0.114).
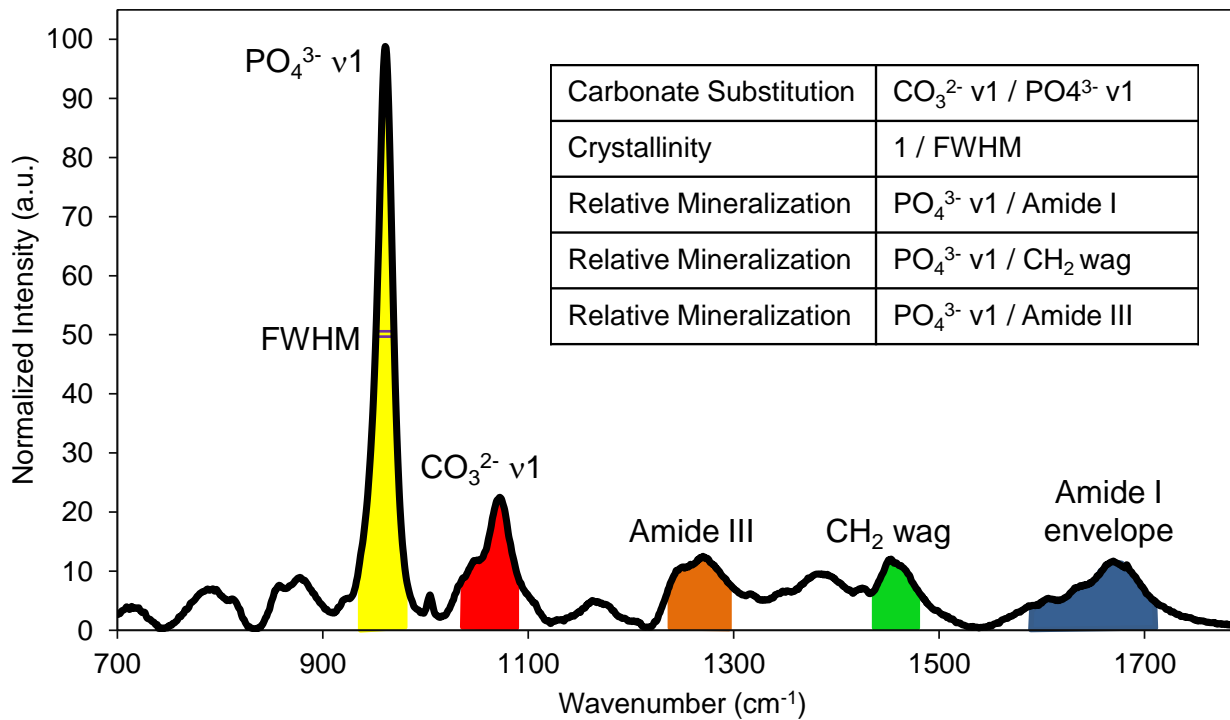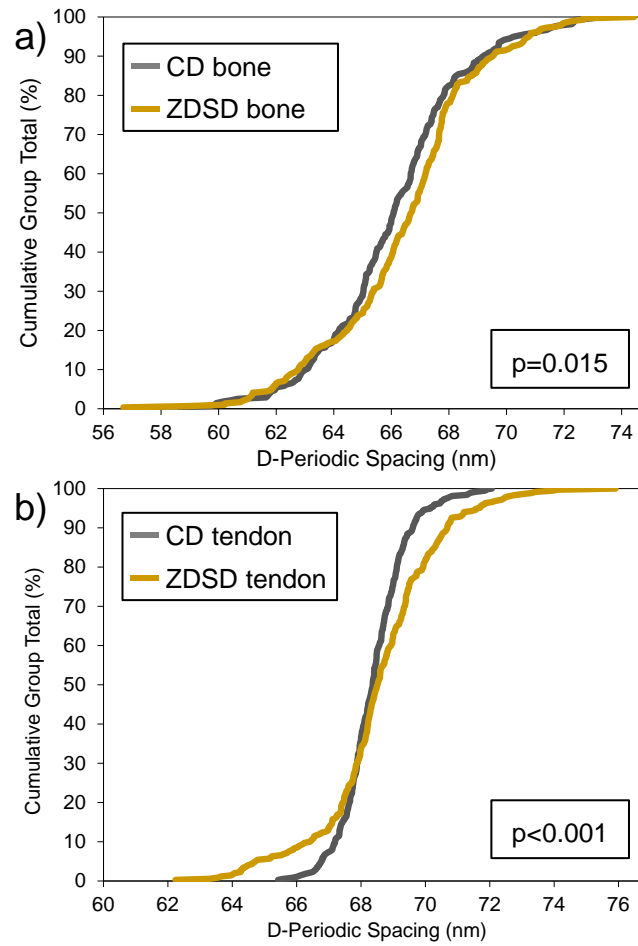
Figure 1

Figure 2

Figure 3

Figure 4

1

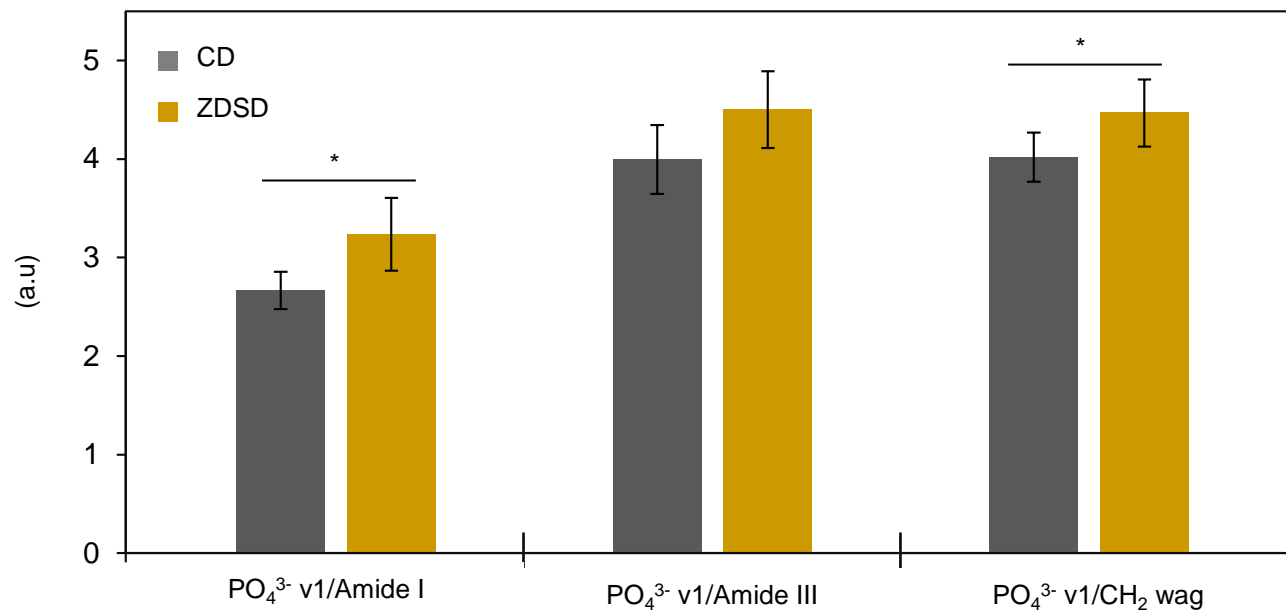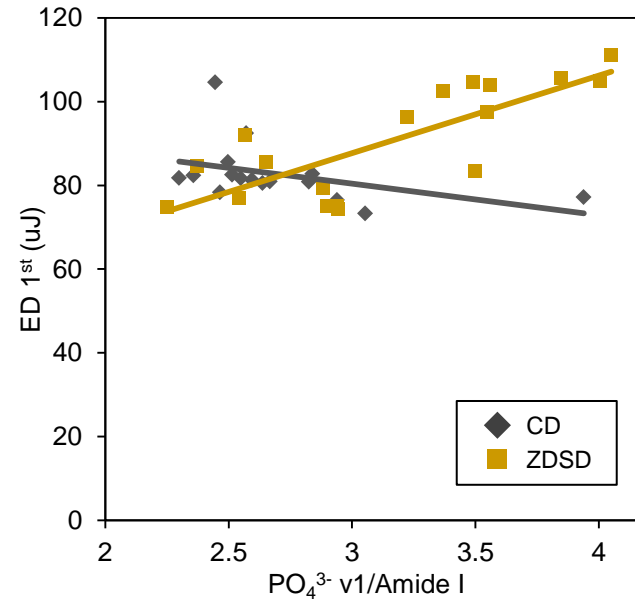## TABLES

Table 1. Animal information at 30 weeks of age.

	CD	ZDSD	p-value
Glucose (mg/dl)	139 ± 8	633 ± 90	**<0.001**
Weight (g)	652 ± 48	490 ± 25	**<0.001**
Hb1Ac (%)	3.32 ± 0.27	8.7 ± 0.72	**<0.001**
Ash Fraction (%)	63.33 ± 0.96	59.81 ± 0.69	**<0.001**
aBMD (g/cm^2)	0.2557 ± 0.0124	0.2093 ± 0.0082	**<0.001**

Values presented as mean ± SD. n=9 per group

Table 2. RPI measurements from proximal tibia.

	CD	ZDSD	ZDSD vs CD	Blocking By Day
ID 1st	43.4 ± 5.3	42.1 ± 5.0	0.316	**<0.001**
ED 1st	80.6 ± 12.8	77.1 ± 11.8	0.188	**<0.001**
US 1st	0.421 ± 0.040	0.423 ± 0.060	0.862	**<0.001**
CID 1st	3.57 ± 0.57	3.23 ± 0.38	**0.010**	**<0.001**
IDI	6.87 ± 1.22	6.27 ± 0.92	**0.040**	**<0.001**
TID	47.5 ± 6.0	45.9 ± 5.5	0.253	**<0.001**
ED Tot	195.2 ± 25.6	189.2 ± 21.2	0.418	**<0.001**
Avg CID	1.30 ± 0.14	1.22 ± 0.10	0.122	**0.002**
Avg ED	11.8 ± 1.7	11.6 ± 1.2	0.730	**0.047**
Avg US	0.437 ± 0.043	0.438 ± 0.064	0.964	**<0.001**

Values presented are mean ± SD for groups and p-values for comparisons. P-values are from a two-way ANOVA with group and day of indentation as the fixed effects. n=9 per group.

Table 3. Raman to RPI correlations in ZDSD.

	ID 1st	ED 1st	US 1st	CID 1st	IDI	TID	ED Tot	Avg CID	Avg ED	Avg US
Crystallinity	-0.023	-0.142	-0.349	-0.046	0.161	0.010	0.291	0.175	0.429	-0.250
CO_3^{2-} v1/ PO_4^{3-} v1	**-0.653***	**-0.559***	-0.202	0.076	0.460	**-0.609***	**-0.475***	-0.039	-0.268	-0.239
PO_4^{3-}v1/ Amide I	**0.770****	**0.791****	0.146	0.347	-0.199	**0.742****	**0.490***	0.377	0.124	0.157
PO_4^{3-} v1/ CH_2 wag	**0.654***	**0.674***	0.046	0.284	-0.067	**0.647***	**0.511***	0.375	0.216	0.073
PO_4^{3-} v1/ Amide III	**0.647***	**0.612***	0.124	0.104	-0.261	**0.623***	**0.604***	0.215	0.375	0.181

Values presented are the Pearson product moment correlation coefficients (r). n=18 locations

* p<0.05, ** p<0.001

23

7. REFERENCES

[1]   National diabetes fact sheet: national estimates and general information on diabetes and prediabetes in the United States, 2011. Centers for Disease Control and Prevention 2011.

[2]   De Liefde I, Van der Klift M, De Laet C, Van Daele P, Hofman A, Pols H. Bone mineral density and fracture risk in type-2 diabetes mellitus: the Rotterdam Study. Osteoporosis International 2005;16: 1713-1720.

[3]   Schwartz AV, Hillier TA, Sellmeyer DE, Resnick HE, Gregg E, Ensrud KE, Schreiner PJ, Margolis KL, Cauley JA, Nevitt MC, Black DM, Cummings SR. Older women with diabetes have a higher risk of falls: a prospective study. Diabetes Care 2002;25: 1749-54.

[4]   Einhorn TA, Boskey AL, Gundberg CM, Vigorita VJ, Devlin VJ, Beyer MM. The mineral and mechanical properties of bone in chronic experimental diabetes. Journal of Orthopaedic Research 1988;6: 317-323.

[5]   Nyman J. Effect of diabetes on the fracture resistance of bone. Clinical Reviews in Bone and Mineral Metabolism 2013;11: 38-48.

[6]   Schwartz AV, Garnero P, Hillier TA, Sellmeyer DE, Strotmeyer ES, Feingold KR, Resnick HE, Tylavsky FA, Black DM, Cummings SR, Harris TB, Bauer DC, for the Health A, Study BC. Pentosidine and increased fracture risk in older adults with type 2 diabetes. Journal of Clinical Endocrinology & Metabolism 2009;94: 2380-2386.

[7]   Merlotti D, Gennari L, Dotta F, Lauro D, Nuti R. Mechanisms of impaired bone strength in type 1 and 2 diabetes. Nutrition, Metabolism and Cardiovascular Diseases 2010;20: 683-690.

[8]   Li Y, Fessel G, Georgiadis M, Snedeker JG. Advanced glycation end-products diminish tendon collagen fiber sliding. Matrix Biology 2013;32: 169-177.

[9]   Siegmund T, Allen MR, Burr DB. Failure of mineralized collagen fibrils: Modeling the role of collagen cross-linking. Journal of Biomechanics 2008;41: 1427-1435.

[10]   Buehler MJ. Molecular nanomechanics of nascent bone: fibrillar toughening by mineralization. Nanotechnology 2007;18: 295102.

[11]   Launey ME, Buehler MJ, Ritchie RO. On the mechanistic origins of toughness in bone. Annual Review of Materials Research 2010;40: 25-53.

[12]   Wallace JM, Erickson B, Les CM, Orr BG, Holl MMB. Distribution of type I collagen morphologies in bone: Relation to estrogen depletion. Bone 2010;46: 1349-1354.

[13]   Fang M, Liroff KG, Turner AS, Les CM, Orr BG, Holl MMB. Estrogen depletion results in nanoscale morphology changes in dermal collagen. Journal of Investigative Dermatology 2012.

[14]   Wallace JM, Orr BG, Marini JC, Holl MMB. Nanoscale morphology of type I collagen is altered in the Brtl mouse model of osteogenesis imperfecta. Journal of structural biology 2011;173: 146-152.

[15]   Erickson B, Fang M, Wallace JM, Orr BG, Les CM, Banaszak Holl MM. Nanoscale structure of type I collagen fibrils: Quantitative measurement of D-spacing. Biotechnology Journal 2013;8: 117-126.

[16]   Gamsjaeger S, Masic A, Roschger P, Kazanci M, Dunlop J, Klaushofer K, Paschalis E, Fratzl P. Cortical bone composition and orientation as a function of animal and tissue age in mice by Raman spectroscopy. Bone 2010;47: 392-399.

[17]   Morris MD, Mandair GS. Raman assessment of bone quality. Clinical Orthopaedics and Related Research 2011;469: 2160-2169.

[18]   Aref M, Gallant MA, Organ JM, Wallace JM, Newman CL, Burr DB, Brown DM, Allen MR. In vivo reference point indentation reveals positive effects of raloxifene on mechanical properties following six months of treatment in skeletally mature beagle dogs. Bone.

[19]   Reinwald S, Peterson RG, Allen MR, Burr DB. Skeletal changes associated with the onset of type 2 diabetes in the ZDF and ZDSD rodent models. American Journal of Physiology-Endocrinology and Metabolism 2009;296: E765-E774.

[20]   Tomasek JJ, Meyers SW, Basinger JB, Green DT, Shew RL. Diabetic and age-related enhancement of collagen-linked fluorescence in cortical bones of rats. Life sciences 1994;55: 855-861.

[21]   Saito M, Fujii K, Mori Y, Marumo K. Role of collagen enzymatic and glycation induced cross-links as a determinant of bone quality in spontaneously diabetic WBN/Kob rats. Osteoporosis International 2006;17: 1514-1523.

[22]   Odetti P, Aragno I, Rolandi R, Garibaldi S, Valentini S, Cosso L, Traverso N, Cottalasso D, Pronzato MA, Marinari UM. Scanning force microscopy reveals structural alterations in diabetic rat collagen fibrils: role of protein glycation. Diabetes/Metabolism Research and Reviews 2000;16: 74-81.

[23]   Kemp AD, Harding CC, Cabral WA, Marini JC, Wallace JM. Effects of tissue hydration on nanoscale structural morphology and mechanics of individual type I collagen fibrils in the Brtl mouse model of osteogenesis imperfecta. Journal of Structural Biology 2012;180: 428-38.

[24]   Wallace JM, Chen Q, Fang M, Erickson B, Orr BG, Banaszak Holl MM. Type I collagen exists as a distribution of nanoscale morphologies in teeth, bones, and tendons. Langmuir 2010;26: 7349-54.

[25]   Fang M, Goldstein EL, Turner AS, Les CM, Orr BG, Fisher GJ, Welch KB, Rothman ED, Banaszak Holl MM. Type I collagen D-spacing in fibril bundles of dermis, tendon, and bone: Bridging between nano- and micro-level tissue hierarchy. ACS Nano 2012;6: 9503-9514.

[26]   Nyman JS, Makowski AJ, Patil CA, Masui TP, O'Quinn EC, Bi X, Guelcher SA, Nicollela DP, Mahadevan-Jansen A. Measuring differences in compositional properties of bone tissue by confocal Raman spectroscopy. Calcified Tissue International 2011;89: 111-122.

[27]   Glenn JV, Beattie JR, Barrett L, Frizzell N, Thorpe SR, Boulton ME, McGarvey JJ, Stitt AW. Confocal Raman microscopy can quantify advanced glycation end product (AGE) modifications in Bruch's membrane leading to accurate, nondestructive prediction of ocular aging. The FASEB journal 2007;21: 3542-3552.

[28]   Dingari NC, Horowitz GL, Kang JW, Dasari RR, Barman I. Raman spectroscopy provides a powerful diagnostic tool for accurate determination of albumin glycation. Plos One 2012;7: e32406.

[29]   Vashishth D, Gibson G, Khoury J, Schaffler M, Kimura J, Fyhrie D. Influence of nonenzymatic glycation on biomechanical properties of cortical bone. Bone 2001;28: 195-201.

[30]   Lapolla A, Fedele D, Martano L, Arico NC, Garbeglio M, Traldi P, Seraglia R, Favretto D. Advanced glycation end products: a highly complex set of biologically relevant

compounds detected by mass spectrometry. Journal of Mass Spectrometry 2001;36: 370-378.

[31] Gallant MA, Brown DM, Organ JM, Allen MR, Burr DB. Reference-point indentation correlates with bone toughness assessed using whole-bone traditional mechanical testing. Bone 2013;53: 301-305.

[32] Indrekvam K, Husby OS, Gjerdet NR, Engester LB, Langeland N. Age-dependent mechanical properties of rat femur: measured in vivo and in vitro. Acta Orthopaedica 1991;62: 248-252.

[33] Zimmermann EA, Schaible E, Bale H, Barth HD, Tang SY, Reichert P, Busse B, Alliston T, Ager JW, Ritchie RO. Age-related changes in the plasticity and toughness of human cortical bone at multiple length scales. Proceedings of the National Academy of Sciences 2011;108: 14416-14421.